SIMULTANEOUS SURFACE AND SUBSURFACE AIR AND WATER FLOWS MODELLING IN THE SWASH ZONE

Jonathan Desombre[1], Denis Morichon[1] and Mathieu Mory[1]

This study presents the results of the numerical simulation of a bore-driven swash flow over a permeable coarse-grained beach, carried out using the THETIS code. This code, based on a VOF-RANS approach, was previously used to simulate the swash flow over an impermeable beach (Desombre et al. 2013). For the present study, the code is extended to account for infiltration and exfiltration into a permeable immobile beach using the Volume-Averaged momentum equation that solves simultaneously the surface and subsurface flows. The results are compared with a laboratory data set from an experiment performed in the swash facility of the University of Aberdeen (Steenhauer et al. 2011). Comparisons between measurements and model results show the ability of the model to simulate the main features of subsurface flow during an entire swash cycle.

Keywords: swash zone; porous media; groundwater; subsurface; numerical modelling; 1-fluid; VOF

INTRODUCTION

The swash zone is considered as one of the most scientifically challenging coastal environment as far as sediment transport is concerned. Sediment transport is in general apprehended as a surface process driven by the flow shear stress applied on the bed. Nevertheless, there are some open questions regarding the interactions between surface and subsurface flows. The influence of infiltration and ex-filtration is twofold. Not only, they can modify the boundary layer thickness (Butt et al. 2001), but the vertical flow also produces a vertical shear stress on the sediment in the bed. Horn (2006) also pointed in her review the poorly understood process of air encapsulation during the wetting of the beach. This encapsulation increases the pore-air pressure, which influences the groundwater flow and is locally capable to reverse the infiltration flow (Steenhauer et al. 2011). Another implication of infiltration is the asymmetry of the surface swash flow. Indeed, as water penetrates inside the beach during run-up, the amount of surface water in the run-down flow can be significantly reduced.

The nature and the magnitude of interactions between surface and ground flows obviously depend on the sediment grain size. The permeability of high grain size beaches (such as gravel) is large and swash flow will result in a significant infiltration into the beach. Reducing the grain size of sediments diminishes the permeability of the soil. The water infiltration into the beach is hence reduced, but exfiltration during run-down is more likely to occur. Additionally, capillary effects, which raises the water level above the water table in fine sediments soils, can no longer be discarded.

In this paper, we investigate by numerical simulation the interactions between the surface swash flow over a permeable beach and the ground flow induced in the porous medium. This is made using the Volume Of Fluid (VOF) code named THETIS. The model presented in this work is based on the Volume-Averaged Reynolds-Averaged Navier-Stokes (VARANS) equations, which are modified to simulate simultaneously the flow in the porous medium by mean of a Darcy-Brinkman-Forchheimer formulation and the flow over the beach of water and air using the Reynolds-Averaged Navier-Stokes (RANS) equations. Currently, the THETIS model does not take into account capillarity effects inside the soil. Simulations were therefore achieved for high grain size sediments (8.5 mm diameter). Taking advantage of recently published laboratory data, the experiment of Steenhauer et al. (2011), who achieved a bore-driven swash event over a coarse-grained permeable immobile beach, was chosen as validation test case.

More recently Steenhauer et al. (2012) compared their laboratory experiments with the results of a numerical model coupling a Non-Linear Shallow Water Equations model (NLSWE) for simulating the surface bore propagation with a conceptual Darcy-Forchheimer ground flow model. This modelling approach is in the continuity of former studies coupling a surface hydrodynamic model with a specific porous flow model. For example, Li et al. (2002) coupled the BeachWin Boundary Element Model (BEM), solving the NLSWE surface wave propagation, with a Darcy model inside the beach and accounting for capillary effects with a specific free surface boundary condition in the saturated beach. Karambas et al. (2003, 2006) coupled a Boussinesq model for surface long wave motions with a porous medium flow model combining a Forchheimer formulation with an added mass inertial term for modelling transient flows. Bakhtyar et al. (2011) coupled a VOF-RANS surface

---

[1] IVS-SIAME, Université de Pau et des Pays de L'adour, 1 Allée du Parc Montaury, Anglet, 64600, France

hydrodynamic model with the subsurface flow module SEAWAT-2000, which models the water table fluctuations due to groundwater flow, using the Darcy law.

As far as VOF modelling is concerned, Hsu et al. (2002) were the first to apply a unique numerical model to study the propagation of a surface wave in front of a permeable composite breakwater. Using the COBRAS code, also based on the VARANS equations, they achieved the closure of the terms resulting from the Volume-Averaging operation inside the porous medium flow by means of a Forchheimer type law with the drag coefficients given by the Engelung (1953) correlation, and of an added mass inertia term. More recently, Lara et al. (2010), in the same framework of the VARANS equations, developed the IH-3VOF code to simulate wave-structure interactions. Higuera et al. (2011) used this code to investigate breaking waves on a gravel slope. Their work focuses on the influence of energy dissipation induced by the porous beach on the free surface evolution and on wave breaking across the surf zone. So far, to the authors' knowledge, no model based on VARANS equations, has been used to simulate ground flow in the swash zone.

In the following, section 2 presents the equations of the THETIS model, focused on simultaneous surface and ground flow modelling. Results of numerical simulations are then compared in section 3 with an extensive set of laboratory data. Conclusions are given in section 4.

NUMERICAL MODEL DESCRIPTION

The THETIS numerical code, developed at the University of Bordeaux (I2M-TREFLE), is extended to simulate simultaneously the surface and subsurface two-phase air-water flows in the swash zone. The model presented here is an extension of the RANS incompressible 1-fluid formulation used by Mory et al. (2011) and Desombre et al. (2013) to simulate dam-break generated swash flows over impermeable beaches. Mory et al. (2011) focused on the aptitude of the THETIS model to simulate the bore collapse and swash flow generation, whereas Desombre et al. (2013) performed a detailed analysis of the swash flow structure over an impermeable beach.

The porous medium is considered at a macro-scale, meaning that the cells meshing the beach soil are Representative Elementary Volumes (REV) with regard to the flow dynamics in the porous medium. The porous medium structure is considered as homogeneous, isotropic and immobile. Thus, the REV parameters, namely the porosity ϕ and the intrinsic permeability k, are constants.

The flow simulation in the porous medium is based on the Forchheimer equation

$$I = a_k \mathbf{v} + b_k \|\mathbf{v}\| \mathbf{v} \qquad (1)$$

which relates the hydraulic gradient I and the Darcy velocity $\mathbf{v}$. This velocity is the volume-averaged velocity over the REV which is linked to the internal pore velocity V by the Dupuit relationship $\mathbf{v} = V \phi$. The linear and quadratic drag coefficients are related to the intrinsic permeability and to the fluid density and viscosity by the respective relations:

$$a_k = \frac{\mu}{\rho g k} \qquad \text{and} \qquad b_k = \frac{\rho C_F}{\rho g \sqrt{k}} \qquad (2)$$

The Forchheimer equation (Eq. 1) is an extension of the Darcy equation. The Darcy equation is valid for modelling low velocity flows in a porous medium, *i.e.* when the Reynolds number based on permeability $\mathrm{Re}_p = \rho \mathbf{v} \sqrt{k} / \mu$ is sufficiently small (*i.e.* $O(1)$), as can be reasonably assumed for sand beaches (Turner and Masselink 1998). However, the flow velocity inside a gravel beach can reach a value such that the Reynolds number is too high and the relationship between the Darcy velocity and the hydraulic gradient is no longer linear. The quadratic drag term in Eq. 1 extends the Darcy law to higher Reynolds flow regime, so called the Forchheimer regime.

The Volume Averaged momentum equation solved by the THETIS numerical model integrates the Darcy-Brinkman-Forchheimer formulation:

$$\rho \left[\frac{1}{\phi} \frac{\partial \mathbf{v}}{\partial t} + \frac{\mathbf{v}}{\phi} . \nabla \frac{\mathbf{v}}{\phi} \right] = -\nabla P + \rho \, \mathbf{g} + \mu_{eff} \nabla^2 \mathbf{v} - \frac{\mu}{k} \mathbf{v} - \frac{\rho C_F}{\sqrt{k}} \|\mathbf{v}\| \mathbf{v} \qquad (3)$$

where $\mu_{eff} = \mu / \phi$ denotes the effective viscosity and C_F the Forchheimer coefficient.

Outside of the porous medium, the porosity is $\phi = 1$ and the intrinsic permeability is set to $k = \infty$. Thereby Eq. 3 reduces to the classical RANS equations. Inside the porous medium, the permeability is low and time-varying flows rapidly evolve toward equilibrium where the Darcy and Forchheimer

terms balance the hydraulic gradient. The Forchheimer equation is recovered when this equilibrium is met. In the porous medium, the left-hand side terms are active during transient evolution and the velocity actually considered is the internal pore velocity. The viscous stress term on the right-hand side, named Brinkman's term, ensures momentum continuity at the surface of the porous medium. Thus, the VARANS equation (Eq. 3) allows solving simultaneously surface and subsurface flows while ensuring continuity at the boundary. The momentum equation is solved assuming incompressibility of the fluid.

$$\nabla . v = 0 \qquad (4)$$

The beach is made of gravels for the simulations presented in this paper. The boundary conditions at the bed surface for the v^2-f turbulence closure model cannot be stated as done at the surface of an impermeable smooth bed (Desombre et al. 2013). Turbulence modelling was therefore discarded for the simulations presented here by equating the eddy viscosity to zero. This has obviously an effect for estimating the bed shear stress applied on the bed, but this topic is not considered in the present paper. On the other hand, since the swash flow is of short duration, neglecting turbulence effects does not modify much the mean velocities and interface displacements, as observed by Mory et al. (2011).

The coupling between velocity and pressure is solved using the two steps pressure-correction method developed by Goda (1978). A provisional velocity is first computed using the momentum equation (Eq. 3) based on the velocity and pressure fields of the previous time step. Then, a correction is applied to the velocity by satisfying incompressibility (Eq. 4).

The Volume Of Fluid code THETIS computes both air and water flows. The 1-fluid formulation of multiphase flow uses a single momentum equation for solving simultaneously air and water flows. The air and water content inside each cell is given by the colour function field $C(x,z,t)$, with $C = 1$ when a cell is filled with water and $C = 0$ when it is filled with air. In each cell the density and viscosity depend on the air and water content

$$\rho = \rho_w C + \rho_a (1-C)$$
$$\mu = \mu_w C + \mu_a (1-C) \qquad (5)$$

ρ_w , μ_w and ρ_a , μ_a are the density and viscosity of water and air respectively.

The VOF-PLIC method is finally implemented in order to determine the evolution of air-water interfaces. In mixed cells ($0<C<1$), the interface is reconstructed by determining the segment separating air and water. The VOF-PLIC method is used to displace the segmented interface (S) by solving the following transport equation:

$$\frac{\partial S}{\partial t} + \frac{v}{\phi} . \nabla S = 0 \qquad (6)$$

The Dupuit relationship appearing in Eq. 6 enables that a wetting front in a dry porous media is displaced with the internal pore velocity V of the fluid. Once the interface has been advected, the new colour function field is computed from the positions of the advected segments. The VOF-PLIC method ensures mass conservation if segments representing air-water interfaces in mixed cells are displaced less than half a cell size during a computational time step. Hence, the model computes automatically the time step of each iteration using a Courant-Friedrichs-Levy (CFL) number less than 0.5.

COMPARISONS OF SIMULATION RESULTS WITH THE LABORATORY TEST CASE OF STEENHAUER et al. (2011)

The test case of numerical simulation was chosen by considering the recent laboratory experiments of Steenhauer et al. (2011), who performed a series of dam-break generated swash experiments over a permeable beach in the long flume at the University of Aberdeen. The experimental set-up consists in an idealised 2D case in which air cannot escape laterally. The configuration is identical to the one used by O'Donoghue et al. (2010) to study swash flow over an impermeable beach. Various beaches were tested. The comparison presented here considers only the experiment performed on the beach made of sediments of 8.5mm median diameter. Those experiments present video measurements of the wetting front propagation throughout the beach. They also provide pressure measurements inside the porous beach.

Numerical set-up

The laboratory experiment of Steenhauer et al. (2011) is simulated by considering the 2D configuration depicted in Fig. 1. The computational domain ranges from $x = -5.82$ m to $x = 6$ m and $z = -0.062$ m to $z = 1$ m. It was discretised in 600×55 uniform cells. The water depth above the bottom is initially 6.2 cm deep, except in a 1 m long and 60 cm deep reservoir containing an amount of water, which is released at time $t = 0$. The rest of the domain is filled with air ($C = 0$). The origin of the coordinate system is placed at the still water level on the 1:10 sloping permeable beach. Numerical time steps are ruled by a CFL condition of 0.2. The beach, made with the 8.5 mm sediments, is modelled as a porous medium with the properties given by Tab. 1
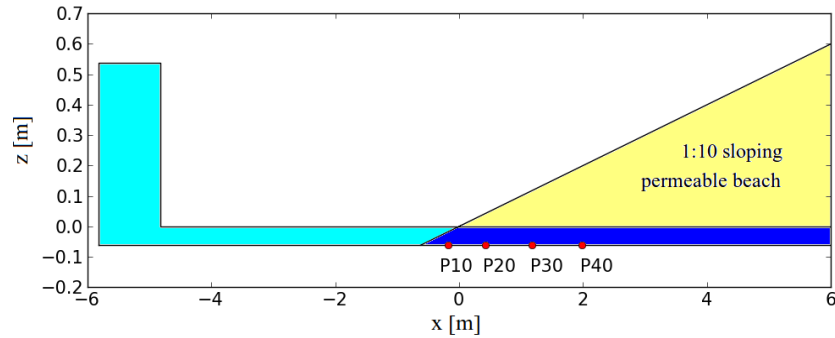
Figure 1. Numerical set-up of Steenhauer et al. (2011) swash event generated by a dam-break on a permeable beach.

Identification of beach properties

Prior to the swash experiment, Steenhauer et al. (2011) characterised the sediment properties by measuring the hydraulic resistance in a constant head apparatus, which consists in a cylinder filled with a sediment layer. The Darcy velocity was measured for several values of imposed hydraulic gradient. The measurements, displayed in Fig. 2, were then fitted to the quadratic Forchheimer law (Eq. 1) from which the linear a_k and quadratic b_k drag coefficients characterising the porous medium were identified. The porosity was also evaluated to $\phi = 0.3$, based on volumetric measurements. Tab. 1 gathers the results of the fitting procedure and the corresponding values of the intrinsic permeability k [m²] and of the Forchheimer coefficient C_F used in THETIS model.

Table 1. Porous beach properties			
a_k	4,1	k	2,48626x10⁻⁸ m²
b_k	383	C_F	0,592435

Fig. 2 also displays the results of numerical simulations by the THETIS model of the relationship between the hydraulic gradient and the Darcy velocity for the constant head conditions of the experiments performed by Steenhauer et al. (2011). The model reproduces perfectly the quadratic relationship between the Darcy velocity and the hydraulic gradient in the porous medium.
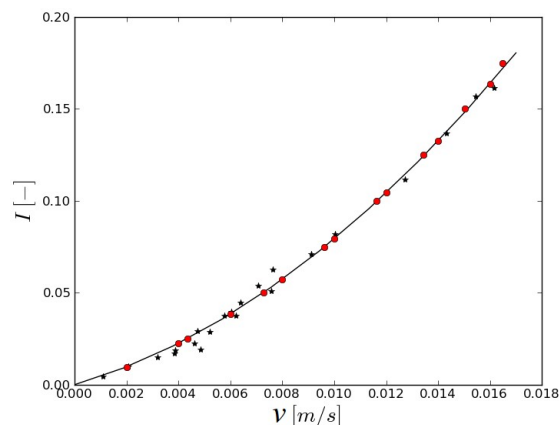

Figure 2. Hydraulic gradient versus Darcy velocity for a layer of 8.5mm diameter sediments obtained by

Steenhauer et al. (2011) from a constant head filtration column experiment. Experimental data are indicated by stars and the quadratic law fitting is the solid line. The dots are the results of the THETIS modelling of the filtration column experiment.

Wetting front

Fig. 3 compares the numerical simulations and the measurements of both surface and subsurface flow profiles at 8 selected instants. The wetting front propagation was obtained by Steenhauer et al. (2011) by subtracting the initial image of the dry beach to the images recorded during swash infiltration through the glass-sided flume. The wetting front positions were then detected by studying contrast differences between dry and wet sand.

In the presented numerical results, the cells containing an air-water interface are coloured in black and coloured in grey when they are filled with water.

We also display the numerical results obtained by Steenhauer et al. (2012) who developed a conceptual model in which the surface flow is described with the NLSWE and the flow in the porous soil with a series of 1D models. Those models were developed to account for relevant flow quantities identified during the experiment (Steenhauer et al. 2011), namely infiltration and ex-filtration, pore-air movement and groundwater flow. Infiltration and ex-filtration, as well as groundwater flow, are simulated using models based on the Forchheimer equation, respectively in a 1D vertical and in a 1D horizontal directions. The air flow inside the beach is considered with a 1D horizontal model derived from the Darcy law.

The comparisons between the numerical results and the measurements indicate that the THETIS model correctly simulates the overall dynamics of the swash lens, but slightly underestimates the maximum run-up. The induced groundwater flow is very well reproduced during the run-up phase, at least until $t = 4$ s. The comparisons show some discrepancies during the run-down phase in particular for the upper part of the wetting front. We attribute those discrepancies to the infiltration front detection method used by Steenhauer et al. (2011), which performs well during the run-up but is less accurate during the run-down phase. Indeed, residual water is kept in the soil when the beach de-saturates. The contrast in images between the saturated and desaturated domains is less visible during run-down, as compared to the contrast seen during run-up between the dry sand and the water saturated sand. The upper boundary of the saturated domain in the beach, hereafter referred as the wetting tail, is thus not well discriminated by the measurements.

For the THETIS model results, the black dots inside the beach indicate that the model enables to simulate the infiltration of bubbles with the water flow through the beach face. While time increases, the number of black dots decreases as bubbles rise towards the surface. Fig. 3 also highlights, that during run-up ($t < 4.5$ s), the most shoreward positions of the surface flow and of the wetting front coincide on the beach surface. During run-down ($t > 4.5$ s), as the water over the beach rapidly retreats seawards while groundwater is retained at higher positions in the beach, a seepage flow occurs between the water exit point (*i.e.* the position where the infiltration front intersects the beach face) and the shoreline. While the model by Steenhauer et al. (2012) reproduces relatively well the surface flow, in particular during the run-up phase, it overestimates the position of the wetting front most of the time.
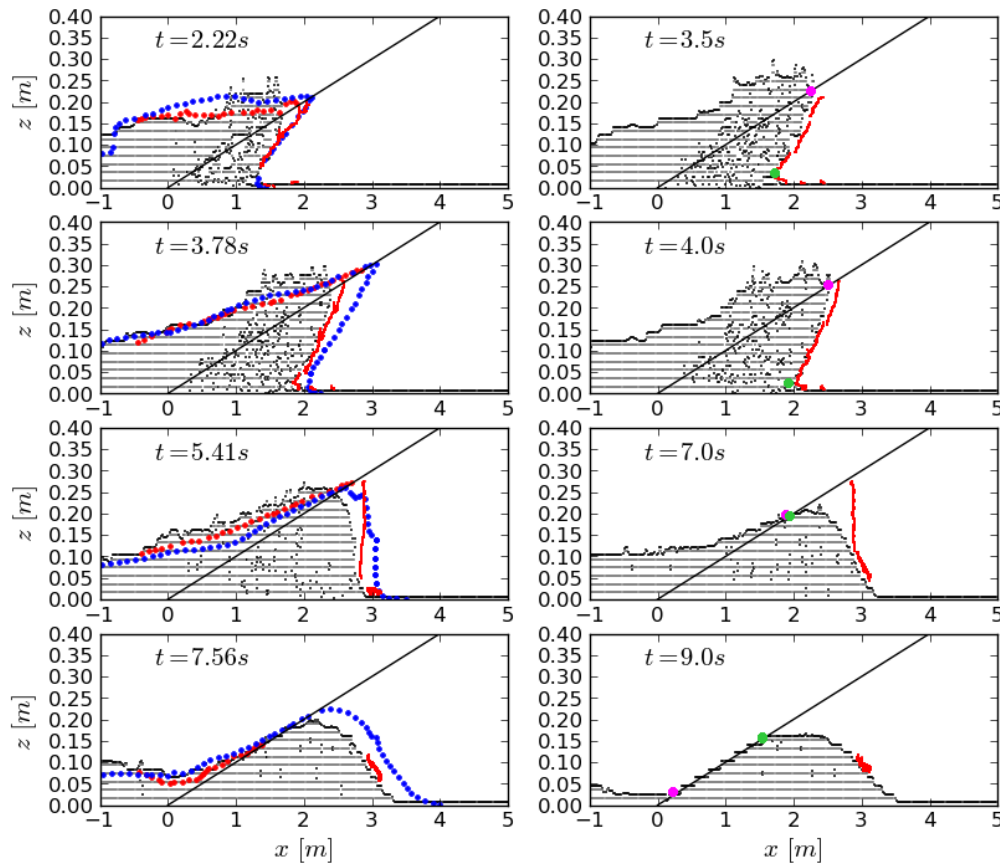
Figure 3. Swash flow profiles measured (red), predicted (blue) by Steenhauer et al. (2012) and simulated by the THETIS model (black).

Infiltrated volume

Steenhauer et al. (2011) estimated during the swash event the variation of the volume of water contained inside the beach by two different methods: (i) by integrating the wetting front profile inside the soil, (ii) by integrating the water depth profile above the permeable beach, which is then subtracted from the initial total amount of water. The measured infiltrated volumes are compared in Fig. 4 with the numerical results obtained with the THETIS model and by Steenhauer et al. (2012).
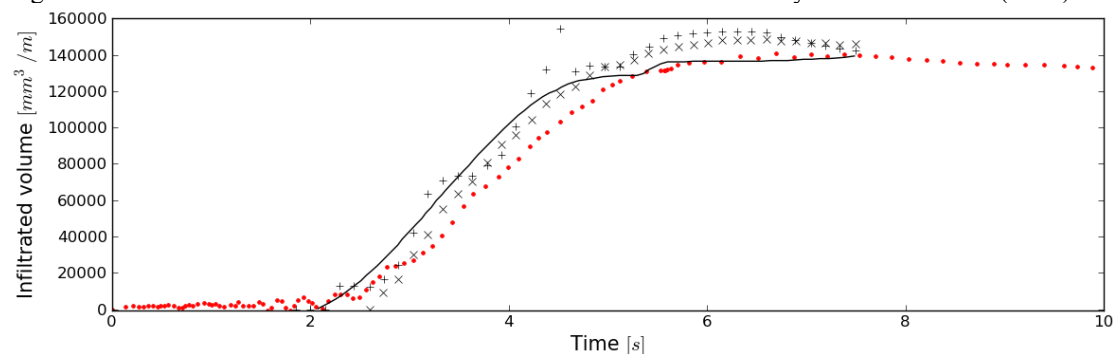
Figure 4. Infiltrated volume of water within the beach during the swash event. Numerical results of the THETIS model (red dots) and of Steenhauer et al. (2012) predictions (solid line). Experimental results based on subsurface (+) and surface (×) measurements.

According to Fig. 4, the THETIS model underestimates the infiltrated volume inside the beach during most of the swash event. It should be noted that in their estimations, Steenhauer et al. (2011) did not consider that air bubbles are entrained in the infiltrated volume of water. Such phenomenon is observed in the results of the THETIS simulations (Fig. 3 and Fig. 7) and the underestimation of our numerical results might then be attributed to the flow aeration in the porous soil. Steenhauer et al.

(2011) mentioned, for their 1.5 mm diameter sediment beach experiment, the release of air from the permeable beach passing through the water layer surface flow. We can reasonably consider that this also occurs for the 8.5 mm diameter sediment beach experiment, as seen in the THETIS numerical simulation. Steenhauer et al. (2012) model slightly overestimates the infiltrated volume of water within the beach during run-up. At the end of the measurements ($t = 7.5\ s$), when bubbles have risen out of the infiltrated water, the results of numerical models and measurements merge. THETIS model results show a very little infiltrated volume loss during late run-down. Most of this loss is due to exfiltration at the beach toe and a small part of it is due to seepage flow. The high grain size of sediment and the high permeability is certainly an important reason for this.
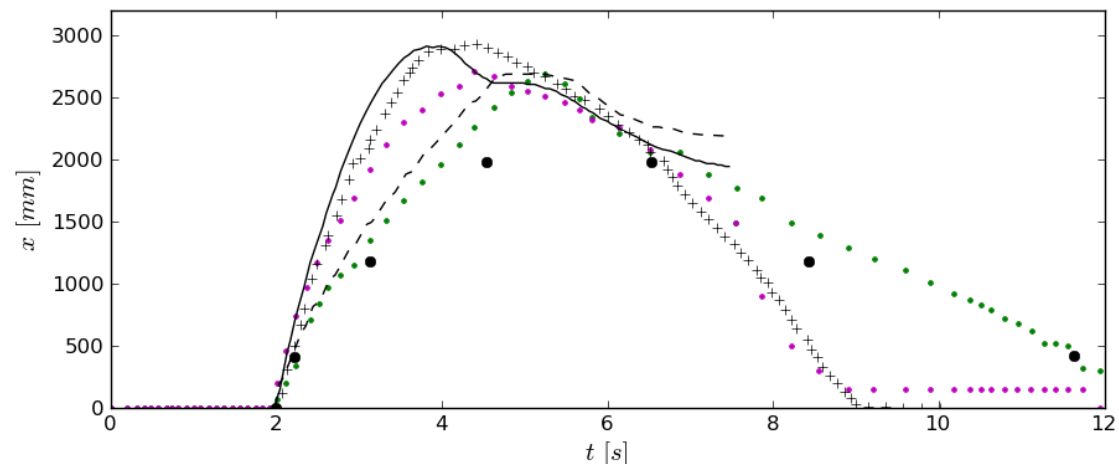

Figure 5. Time-series of the shoreline and saturation boundary positions. Measured (+ and ●) and predicted (solid and dashed lines) by Steenhauer et al. (2011,2012) and simulated by the THETIS model (purple and green dots). For each class, the two symbols refer to the shoreline and the saturation boundary positions, respectively.

Shoreline position and saturation boundary

Fig. 5 compares the time-series of predicted and measured shoreline and saturation boundary positions. The saturation boundary inside the beach was defined by Steenhauer et al. (2011) as the most inshore position where the beach is fully saturated along a vertical. In other words, during most of the run-up, the saturation boundary corresponds to the intersection between the wetting front and the water table. During run-down, it coincides with the water exit point position. To illustrate the definitions of the shoreline and saturation boundary, their positions determined from our simulations are marked on the right panels of Fig. 3 by purple and green dots, respectively.

Confirming the observations in Fig. 3, Fig. 5 shows that the THETIS model underestimates the maximum run-up length but predicts a displacement of the shoreline position during run-down, which is very close to the measured values. Contrariwise, the surface module of Steenhauer et al. (2012) simulates reasonably well the run-up phase but overestimates the shoreline position during run-down.

The overall evolution of the saturation boundary positions during the entire swash event is well reproduced by the THETIS model, although the computed positions are slightly shoreward than the measurements. The discrepancies are more important for the numerical results of Steenhauer et al. (2012). This was expected since their model tends to overestimate the wetting front propagation inside the beach (Fig. 3). Considering simultaneously the shoreline and the saturation boundary positions allows discussing the seepage phenomenon during the run-down phase. Since the saturation boundary is the water exit point during run-down, the domain between the shoreline position and the saturation boundary corresponds to the seepage surface length. Results presented in Fig. 5 show that a seepage surface appears at $t \sim 6.5\ s$ and develops until the shoreline reaches the beach toe. At this time ($t \sim 9.0\ s$), the seepage surface length is almost half of the maximum run-up length. This time evolution of the seepage surface, which reflects the very slow motion of the water in the porous soil compared to the surface flow, is well reproduced by the THETIS model.
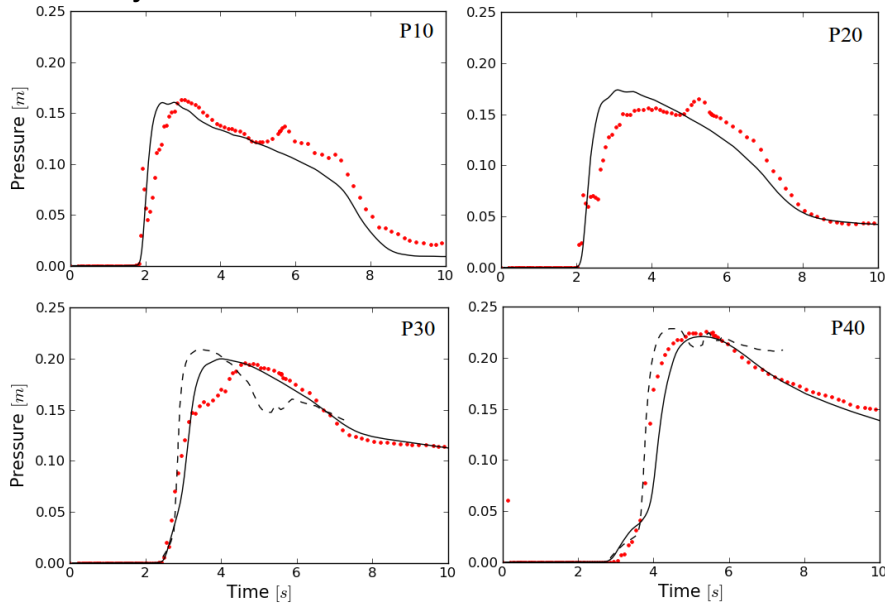
Pressure and velocity fields

Figure 6. Time series of the hydraulic head [m] measured (solid line) at 4 locations inside the beach, compared with the THETIS simulation results (red dots) and Steenhauer et al. (2012) model predictions (dashed line). P10 at x = -0.18m, P20 at x = 0.42m, P30 at x = 1.18m and P40 at x = 1.98m.

In Steenhauer et al. (2011) experiments, pressure sensors were placed at the bottom of the permeable beach, as indicated in Fig. 2. Fig. 6 compares four measured time-series of the hydraulic head with the results of simulations obtained by the THETIS model. For pressure sensors P30 and P40 the numerical results of Steenhauer et al. (2012) are also displayed. Fig. 6 shows a steep increase of the hydraulic head at P10 ($t \approx 1.8$ s) and at P20 ($t \approx 2$ s) when the wetting front reaches the water table. At positions further inshore, a smaller rate of increase precedes the steep increase of the wetting front arrival, particularly visible for P40. This is mainly due to the groundwater flow generated by the infiltrated water at the lower end of the beach and by the air encapsulation between the wetting front and the water table. Once, the wetting front has fully connected the water table, the hydraulic head decreases as the water level above the sensor decreases. The overall agreement between our model and the measurements is quite good. The underestimation of the hydraulic head by the model around the time of maximum pressure, especially visible for P30, is attributed to the aeration of the infiltrated water. Once the infiltrating flow has reached the groundwater level and bubbles have raised towards the surface, the predicted hydraulic head approaches the experimental values. Numerical results of Steenhauer et al. (2012) also show an overall good agreement with experimental data. However, the results of the THETIS model present unexplained oscillations of the hydraulic head during decay.
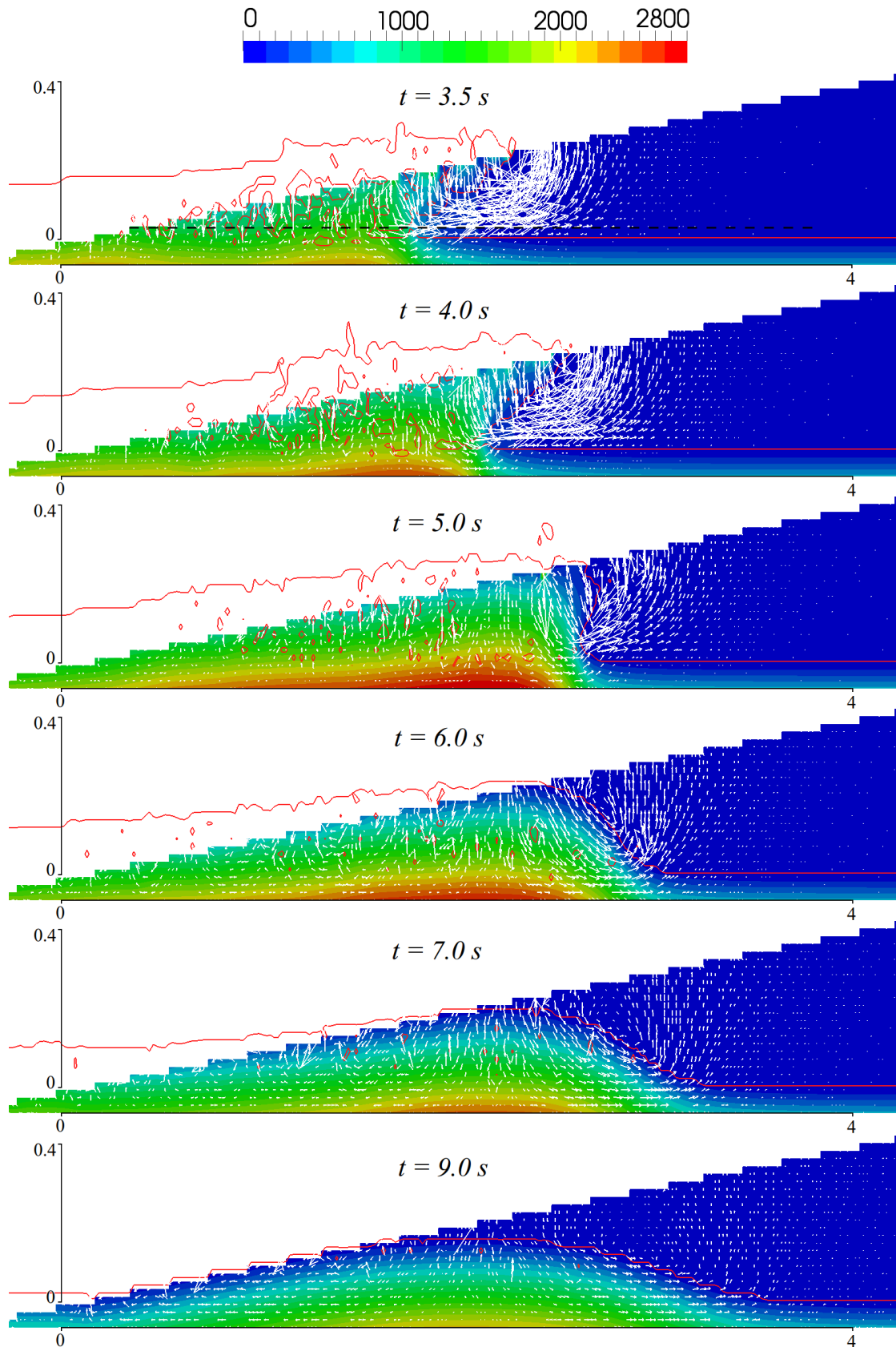
Figure 7. Pressure [Pa] (colour map) and velocity (white vectors) fields inside the beach computed by the THETIS model at 6 times during the swash event. The red solid line represents air-water interfaces.

Fig. 7 presents the pressure and velocity fields plotted from THETIS model results for 6 times during the swash event. The air-water interfaces and the velocity vectors are superimposed. For readability, the scale of the velocity vectors is doubled in the three last frames. The numerical results show that, during run-up ($t < 4.5$ s), the aerated swash flow generated by the dam-break partially infiltrates in the initially dry beach. The infiltration flow between the beach surface and the wetting front is mainly vertical, which is consistent with the 1D vertical modelling considered in Steenhauer's model.
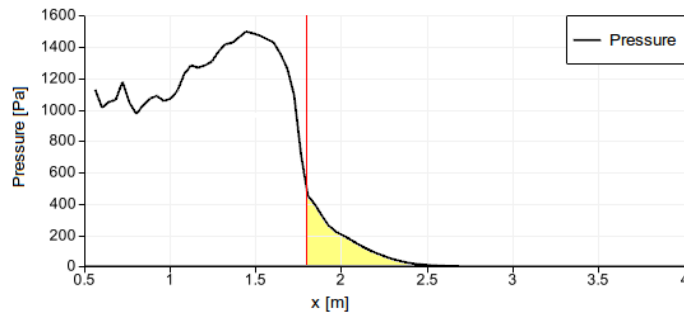

Figure 8. Horizontal pressure [Pa] profile inside the beach 4cm above groundwater level at $t = 3.5$s.

Fig. 8 shows, at $t = 3.5$ s, the horizontal pressure profile inside the beach just above the water table (*i.e.* along the dashed line at $z = 4$ cm on Fig. 7 upper panel). As the red line delineates the position of the air-water interface, the yellow area highlights the increase of pore-air pressure caused by the encapsulation of air between the wetting front and the water table, as previously mentioned. As described by Steenhauer et al. (2011), this additional pore-air pressure generates a horizontal pressure gradient and thus a horizontal air flow directed shoreward. THETIS simulations highlights that air chased by the wetting front rapidly moves upwards and finally escapes vertically out of the porous soil just in front of the swash lens as depicted in Fig. 7.

During run-down ($t > 4.5$ s), Fig. 7 shows that the computed wetting front is fully connected with the water table and that ground air flow is mainly vertical. At positions where there is no more water over the bed, the upper part of the beach starts to de-saturate below the beach face. Inside the beach, the wetting tail forms a groundwater bulge that spreads in a diverging flow. This diverging flow causes little seaward ex-filtration at the toe of the beach and a shoreward expansion of the water table level. Then, a small seepage flow runs down the beach from the water exit point.
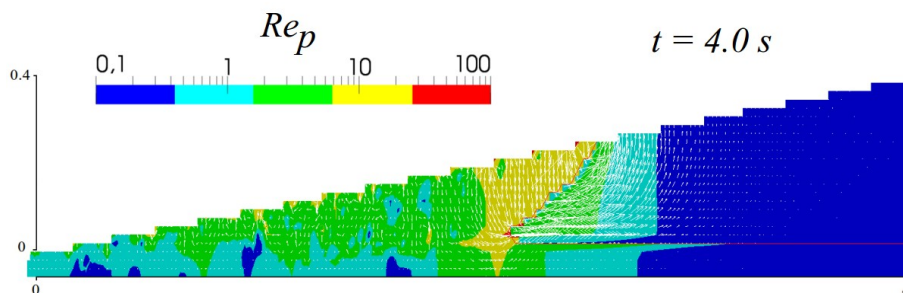

Figure 9. Reynolds number Re_p field in the beach at $t = 4.0$s.

Fig. 9 displays the values of the Reynolds number inside the beach at $t = 4.0$ s. The figure highlights that groundwater flow at the rear and above the wetting front is in the Forchheimer regime (i.e. $Re_p > O(1)$), while the rest of the flow mainly remains in a Darcy regime. Those observations were verified during the entire run-up phase. Analysing THETIS model results shows that regarding the Reynolds number of the air flow inside the beach, it could be considered that it always remains in Darcy regime during the experiment as considered in Steenhauer et al. (2012) model.

CONCLUSION

In this study, the THETIS model was extended to simulate an unsteady bore-driven swash flow over of a coarse-grained permeable immobile beach. Both the flows of water and air are computed simultaneously over and inside the beach. Comparisons with a laboratory experiment by Steenhauer et al. (2011) were performed to assess the ability of the model to simulate the relevant processes of ground flow in the swash zone.

In particular, the model simulates the wetting front propagation during the entire swash cycle, including the development of a wetting tail during the de-saturation of the beach. The appearance and the evolution of a seepage area on the beach surface during the run-down phase is also well reproduced. The model simulates the pore-air pressure increase and the horizontal flow due to encapsulation during infiltration. It also reveals that air is released vertically just in front of the surface swash lens. Values of Reynolds numbers inside the beach indicate that the groundwater flow above and behind the wetting front is in the Forchheimer regime, whereas the air flow generated in the beach is in the Darcy regime.

The presented model has also been compared with a conceptual model developed by Steenhauer et al. (2012), coupling a surface and subsurface module. The THETIS model provides new insights, in particular regarding the role of the subsurface air flow, and is more accurate, for the test case considered, for predicting the wetting front displacement inside the soil.

In future work, we intend to extend the model to simulate ground flow for beaches made of fine sand sediments. This implies to account for the matrix potential, *i.e.* surface tension forces which are responsible of capillary effects. The paper by Steenhauer et al. (2011) includes a laboratory set of data for a beach made of 1.5 mm diameter sediments, for which a 50 mm depth capillary fringe was measured. Since the THETIS model does not include capillary effects, we restricted our simulations to the 8.5 mm diameter sediments experiment, for which no capillary fringe is observed. Addressing the cases of finer sediment beaches is nevertheless an important issue for beaches coastal morphodynamics.

ACKNOWLEDGMENTS

REFERENCES

Bakhtyar, R., A. Brovelli, D.A. Barry and L. Li . 2011. Wave-induced water table fluctuations, sediment transport and beach profile change: Modeling and comparison with large-scale laboratory experiments . *Coastal Engineering*, 58, 103-118.

Butt, T., P.E. Russel, and I.L. Turner. 2001. The influence of swash infiltration-exfiltration on beach face sediment transport: onshore or offshore ?, *Coastal Engineering*, 42, 35-52.

Desombre, J., M. Morichon, and M. Mory. 2013. RANS v²–f simulation of a swash event: Detailed flow structure, *Coastal Engineering*, 71, 1-12.

Goda, K. 1978. A multistep technique with implicit difference schemes for calculating two- or three-dimensional cavity flows. *Journal of Computational Physics*, 30, 76-95.

Higuera, P., J.L. Lara, M. del Jesus, I.J. Losada, Y. Guanche and G. Barajas. 2011. Numerical simulation of three dimensional breaking waves on a gravel slope using two-phase flow Navier-Stokes model. *Proceeding of 5th International Conference on Advanced COmputational Methods in ENgineering* (ACOMEN), 10 pp.

Hoque, Md. and T. Asano, 2007. Numerical study on wave-induced filtration flow across the beach face and its effects on swash zone sediment transport. *Ocean Engineering*, 34, 2033-2044.

Horn, D. 2006. Measurement and modelling of beach groundwater flow in the swash-zone: a review, *Continental Shelf Research*, 26, 622-652.

Hsu, T.J., T. Sakakiyama and P.L.F. Liu. 2002. A numerical model for wave motions and turbulence flows in front of a composite breakwater. *Coastal Engineering*, 46, 25-50.

Karambas, T.V. 2003. Modelling infiltration-exfiltration effects on cross-shore sediment transport in the swash zone. *Coastal Engineering Journal*, 45, 63-82.

Karambas, T.V. 2006. Prediction of sediment transport in the swash zone by using a nonlinear wave model. *Continental Shelf Research,* 26, 599-609.

Lara, J., I.J. Losada, M. del Jesus, G. Barajas and R. Guanche. 2010. IH-3VOF: A three-dimensional Navier-Stokes model for wave and structure interaction. *Proceedings of 32th the International Conference on Coastal Engineering*.

Li, L., D.A Barry, C.B Pattiaratchi and G. Masselink. 2002. BeachWin: modeling groundwater effects on swash sediment transport and beach profile changes. *Environ. Model. Softw*. 17, 313-320.

Mory, M., Abadie, S. Mauriet, and P. Lubin. 2011. Run-up flow of a collapsing bore over a beach, *European Journal of Mech. B/Fluids*, 30, 565-576.

Nield, D.A. 1991. The limitations of the Brinkman-Forchheimer equation in modeling flow in saturated porous medium and at interface. *Int. J. Heat and Fluid Flow*, 12, 269-272.

Nield, D. A. and A. Bejan. 2006. Convection in Porous Media, *SPRINGER*, 3rd ed.

O'Donoghue, T., D. Pokrajac and L.J. Hondebrink. 2010. Laboratory and numerical study of dambreak generated swash on impermeable slopes. *Coastal Engineering*, 57, 513-530.

Steenhauer, K., D. Pokrajac, T. O'Donoghue, and G.A. Kikkert. 2011. Subsurface processes generated by bore-driven swash on coarse-grained beaches, *Journal of Geophysical Research*, 116, 17pp.

Steenhauer, K., D. Pokrajac and T. O'Donoghue. 2012. Numerical model of swash motion and air entrapment within coarse-grained beaches, *Coastal Engineering*, 64, 113-126.

Turner I.L. and G. Masselink. 1998. Swash infiltration-exfiltration and sediment transport. *Journal of Geophysical Research*, 103, 813-824.

Vafai, K. and S. J. Kim. 1995, On the limitations of the brinkman-forchheimer-extended darcy equation, *Int. J. Heat and Fluid Flow*, 16, 11-15.